PATTERN COMPETITION IN HOMOGENEOUSLY HEATED FLUID LAYERS

G. M. Cartland Glover[1], S. C. Generalis[2]
[1]Institute of Safety Research, Forschungszentrum Dresden-Rossendorf, Dresden, Germany
[2]Aston University, Birmingham, United Kingdom

Abstract

Simulations examining pattern competition have been performed on a horizontal homogeneously heated layer that is bounded by an isothermal plane above an adiabatic plane. Several different circulation patterns arose as the heating regime applied to the horizontal layer was modified. The sequence of the patterns formed as the Grashof number was increased had the following order: laminar, z-axis rolls, squares, hexagons and pentagons, pentagons and then two different square modes of differing orientations. Fourier analysis was used to determine how the key modes interact in the presence of different patterns.

Nomenclature

c_p	specific heat capacity at constant pressure (J kg^{-1} K^{-1})	e	internal energy (J kg^{-1})
Gr	Grashof number (-)	Gr_c	critical Grashof number = 197.71 (-)
$\mathbf{g}$	acceleration due to gravity (m s^{-2})	k	thermal conductivity (W m^{-1} K^{-1})
L	characteristic length (m)	Pr	Prandtl number (-)
p	pressure (kg m^{-1} s^{-2})	Ra	Rayleigh number (-)
$\mathbf{S}$	momentum source terms (kg m^{-2} s^{-2})	$\dot{S}$	energy source terms(kg m^{-1} s^{-3})
$\dot{S}_i$	internal heat source (kg m^{-1} s^{-3})	T	temperature (K)
T_r	reference temperature (K)	t	time (s)
$\mathbf{u}$	velocity vector, $[u, v, w]$ (m s^{-1})	$\mathbf{x}$	position vector, $[x, y, z]$ (m)
α	thermal diffusivity (m^2 s^{-1})	β	expansion coefficient (K^{-1})
ϵ	reduced Grashof number (-)	μ	dynamic viscosity (kg m^{-1} s^{-1})
ν	kinematic viscosity (m^2 s^{-1})	ρ	density (kg m^{-3})

1 Introduction

The numerical simulation of the early stage transition regime of an internally heated convective flow has importance in the development of flows found in engineering and geophysical situations. Examples of such convection processes include flows driven by density differences arising from heat generated by the radioactive decay of elements in the Earth's mantle (Houseman, 1988; Schmalzl et al., 1995; Schubert et al., 1993) and in nuclear reactors (Asfia and Dhir, 1996), from biochemical and chemical reactions or from the application of electric currents to conducting fluids (Roberts, 1967; Tritton and Zarraga, 1967). To help understand the formation of the flow structures generated, simulations have been performed on a horizontal layer at a Prandtl number of 7.

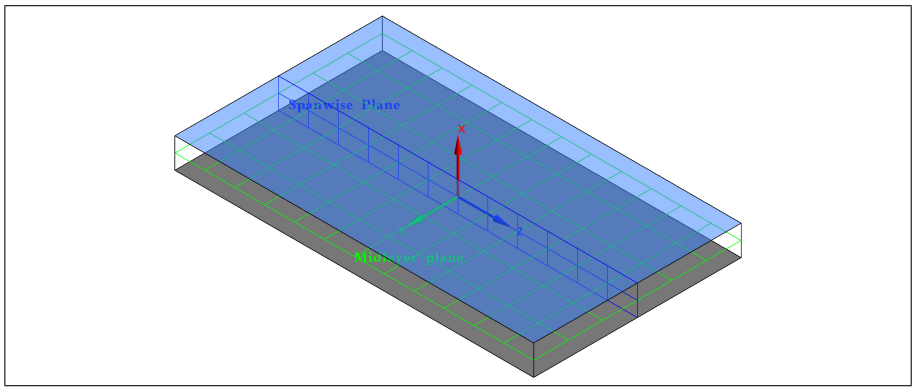

Figure 1: *Diagram of the homogeneous layer with an isothermal surface above an adiabatic surface. The coordinate axis at the origin and the midlayer and spanwise planes are also indicated.*

2 Theory

A rectangular layer that has an aspect ratio of $\left[1 : 4\sqrt{3} : 12\right]$ was defined according to Ichikawa et al. (2006) where the respective resolution of $[30 : 104 : 180]$ was used to simulate the cellular convective flow of an incompressible fluid (Figure 1). The flow was resolved by the conservation equations of mass (1a), momentum (1b) and thermal energy (1c) using the solver, ANSYS CFX (ANSYS, 2007), where an earlier form of the solver successfully modelled convection rolls in an isothermally bounded cavity (Arter et al., 1987).

$$\frac{\partial \rho}{\partial t} + \nabla \cdot (\rho \mathbf{u}) = 0 \tag{1a}$$

$$\frac{\partial \rho \mathbf{u}}{\partial t} + \nabla \cdot (\rho \mathbf{u} \otimes \mathbf{u}) = \nabla p + \nabla \cdot \mu \left[\nabla \mathbf{u} + (\nabla \mathbf{u})^T\right] - \mathbf{g}\rho_c \beta \left(T - T_c\right) + \mathbf{S} \tag{1b}$$

$$\frac{\partial \rho e}{\partial t} + \nabla \cdot (\rho \mathbf{u} e) = \nabla \cdot (\lambda T) + p \nabla \cdot \mathbf{u} + \mu \left[\nabla \mathbf{u} + (\nabla \mathbf{u})^T\right] : \nabla \mathbf{u} + \dot{S} \tag{1c}$$

Where e, p, T, t and $\mathbf{u}$ are the internal energy, pressure, temperature, time and the fluid velocity vector. The fluid properties are defined by the specific heat capacity at constant pressure, c_p, thermal conductivity, k, dynamic viscosity, μ and the density, ρ. The terms, $\mathbf{S}$ and $\dot{S}$ introduce the momentum and energy source terms into the respective transport equations. β is the expansion coefficient and $\mathbf{g}$ is the acceleration due to gravity.

The boundary conditions applied to the planes above and below internally heated layer, were an isothermal plane ($T = T_r$)above an adiabatic plane ($\frac{\partial T}{\partial \mathbf{x}} = 0$). The remaining boundaries between the planes are defined as periodic conditions in order treat the planes as two infinitely sized boundaries.

The Grashof number with the form $Gr = \mathbf{g}\beta \dot{S}_i L^5 / 2\nu^2 k$ was used to control the value of internal heat source applied to the horizontal layer. Where $\dot{S}_i$ and L are the internal heat source and the width of the layer, whilst $\nu = \mu/\rho$ is the kinematic viscosity and $\alpha = k/c_p\mu$ is the thermal diffusivity. Note that $\dot{S}_i$ was estimated by assuming a temperature difference across the layer and then adjusting the characteristic length to give different $\dot{S}_i$ and therefore Gr.

The Prandtl number, $Pr = \nu/\alpha$, has been shown to have little influence on critical limit of Gr that could be correlated over the range $0.1 < Pr < 35$ for inclined homogeneous heated flows between two isothermal planes (Generalis and Nagata, 2003; Gershuni et al., 1974). Thus, a Pr of 7 was selected to avoid a strong influence of the thermal diffusivity on the critical limit of Gr, where the product, $GrPr$, gives the Rayleigh number, Ra, another measure of the stability of cellular convective flows.

3 Results and Discussion

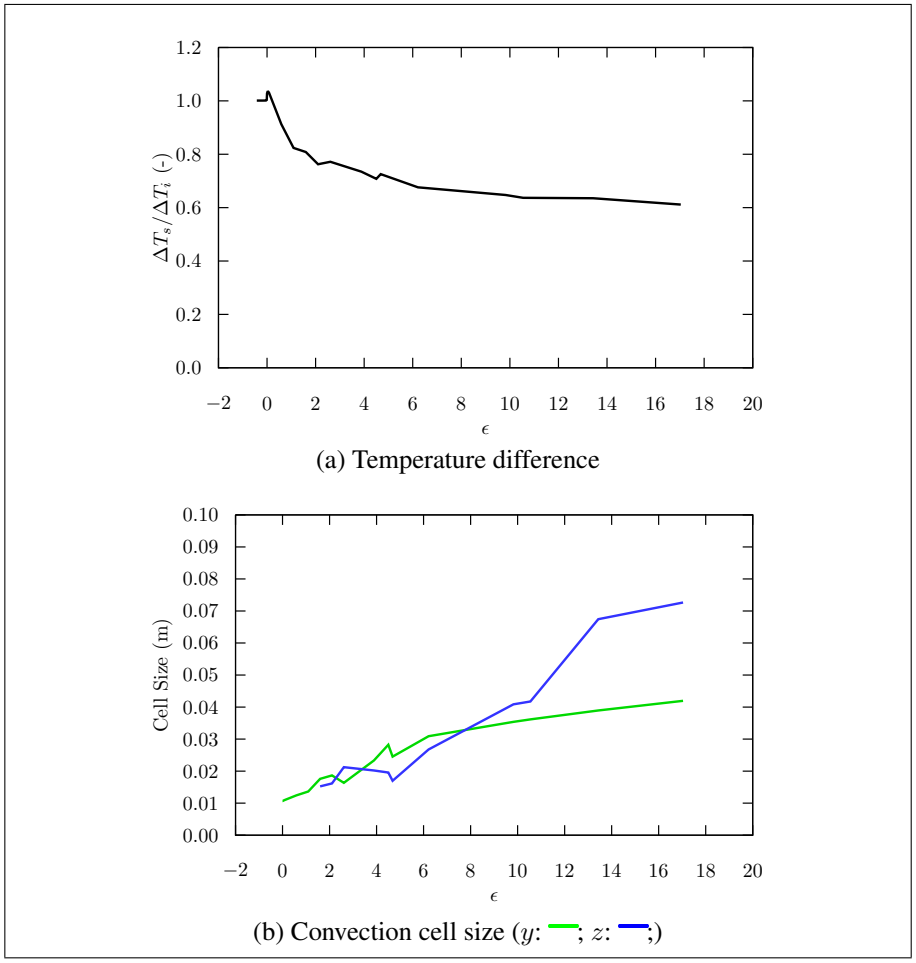

(a) Temperature difference

(b) Convection cell size (y: ; z: ;)

Figure 2: *Profiles of the non-dimensionalised temperature difference and circulation cell size as the value of* ϵ *is increased*

For the case of the internally heated layer with an isothermal plane above an adiabatic plane, $\epsilon = (Gr - Gr_c)/Gr_c$ was increased from -0.42 to 17 where $Gr_c = 197.71$ or the critical value of Ra that was reported as 1386 by Ichikawa et al. (2006). The resultant solutions for the convection initially take the form of a laminar layer, which is then disturbed by the circulation cells that are formed when $\epsilon > 0$ as indicated by the change in characteristic parameters plotted in Figures 2 and 3. Figure 2 presents the non-dimensionalised temperature difference (Figure 2a) and the increase in the approximate circulation cell size (Figure 2b), whilst Figure 3 presents the non-dimensionalised velocity components (Figure 3a) and the first six Fourier space modes (Figure 3b).

The stable structures are formed in the following sequence: longitudinal rolls then squares, hexagons, pentagons and again squares; however the squares have different orientations as depicted in Figures 4 and 5. Note that when $\epsilon \gg 17$ the heated layer becomes unstable, which corresponds to the range of ϵ for stable hexagonal circulation cells reported by Tveitereid and Palm (1976) for the case of internal heated convection in a similarly bounded horizontal layer. This is despite the formation of several different patterns in the current study, which were also indicated in the analysis of Roberts (1967).

The evolution of the temperature (Figure 2a) has a peak at $\epsilon = 0$, which is then followed by an asymptotic decrease as ϵ is increased. The temperature difference is consistent with those reported by Ichikawa et al. (2006) at $\epsilon \approx 2.6$. Note that the heat flux through the upper isothermal boundary was up to about -300 W m^{-2}, which may be the cause of the deviation in the temperature difference

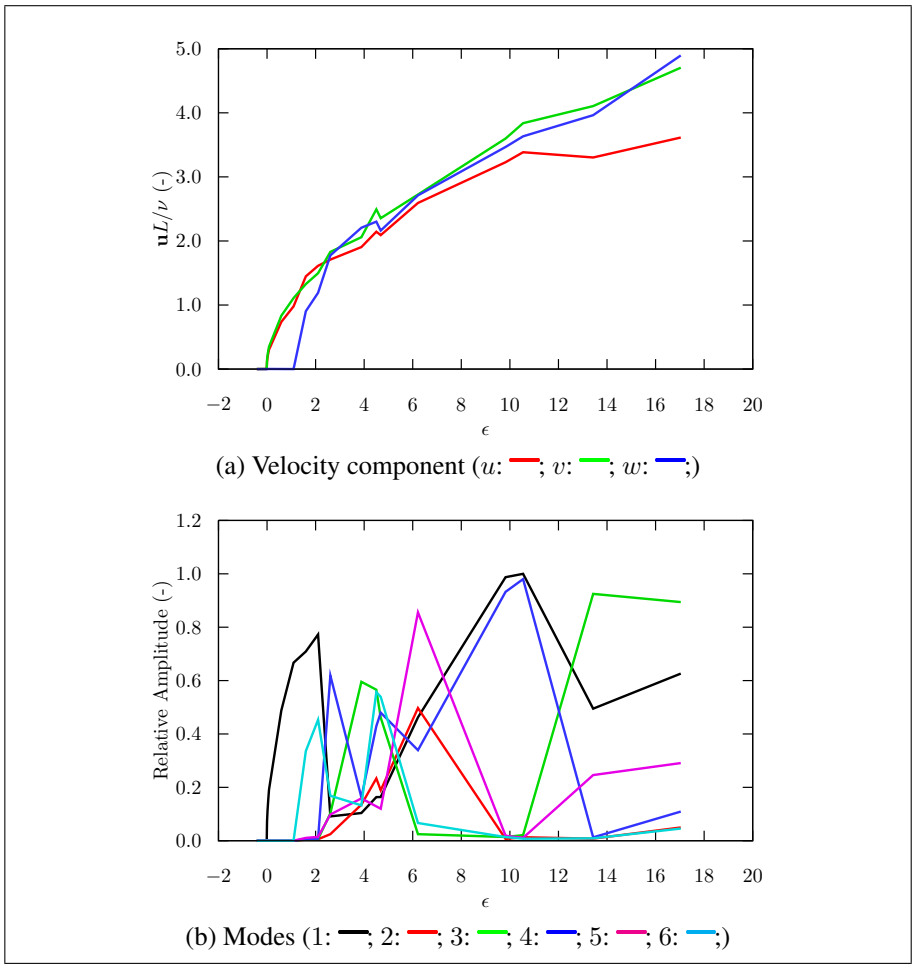

(a) Velocity component (u: ; v: ; w: ;)

(b) Modes (1: ; 2: ; 3: ; 4: ; 5: ; 6: ;)

Figure 3: *Profiles of the non-dimensionalised velocity components and the relative amplitude of the first six modes in Fourier space as the value of* ϵ *is increased*

from the laminar state observed in Figure 2a. At the same time that there is a change in the temperature profile, the size of various circulation cells that are formed are indicated in Figure 2b. The cells increase in size as ϵ is augmented and are comparatively stretched along the z-axis when $\epsilon \gg 6$. Note that at $\epsilon = 3.9$ and 4.7, the value of Pr was slightly less than the specified value of 7. This had no significant impact on the temperature, cell sizes, velocity components or the Fourier modes as ϵ is augmented in the profiles observed in Figures 2 and 3. Especially as the resolved flow field at $\epsilon = 4.5$ gave the same distribution of the circulation cells to those observed at $\epsilon = 4.7$, where the distribution can be seen in the temperature and u velocity component contours presented in Figures 4h and 5h.

The velocity components depicted in Figure 3a display a significant increase in the u and v velocity components at $\epsilon = 0$; however the w velocity component does not increases until $\epsilon > 1.1$ and again at $\epsilon > 2$. The increases in velocity are respectively associated with changes in the state of the fluid layer (see also Figures 4 and 5), from z-axis rolls to squares to what could be considered isotropic hexagons (Groh et al., 2007). However, Groh et al. (2007) stated that hexagons are isotropic in two dimensions, which is not the case in this study as the hexagons are isotropic in all three spatial dimensions. The velocities become anisotropic at values of $\epsilon \gg 6$ as the velocities lose their similarity and there is a concurrent change in the flow state and the circulation cells are stretched along the z-axis.

Therefore, a Fourier analysis of u velocities estimated in the midlayer plane (Figure 1) was performed to identify the significant modes that categorise the different states. Fourier space modes have long been used in the description and prediction of the formation rolls, hexagonal and squares in various

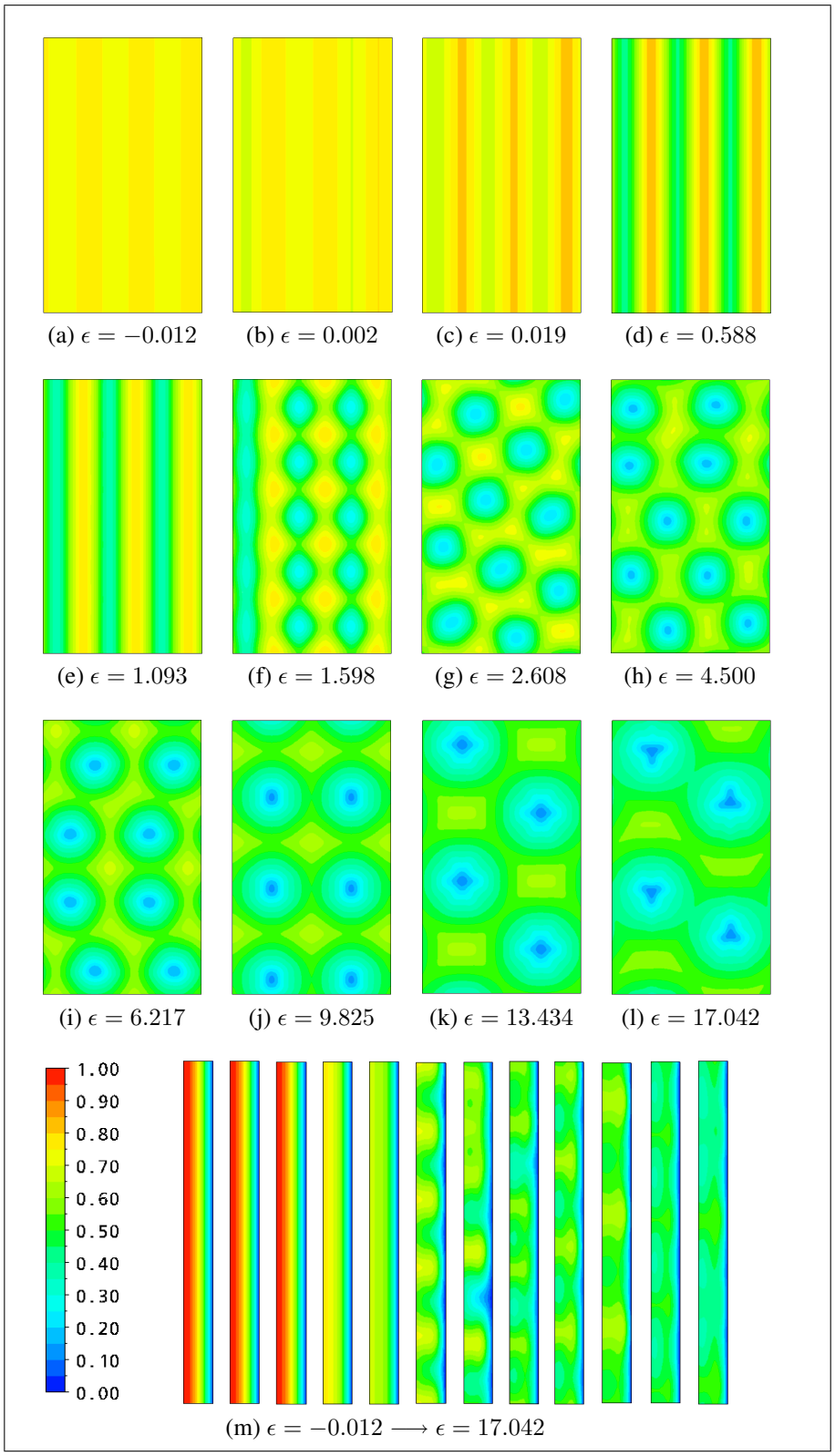

Figure 4: *Temperature contours on the midlayer and spanwise planes in Figure 1.*

forms of thermal convection. The technique first introduced by Busse (1967) was applied recently in the analysis of rolls and hexagonal cells in an experimental study of convection in a so-called *ferrofluid* that was driven by two magnetic fields at right angles to one another (Groh et al., 2007). A new saddle node bifurcation was identified by (Groh et al., 2007) as a result of this analysis that bridges hexagons and stripes. In the study performed here, the relative amplitude of the first six Fourier space modes are found to vary with ϵ.

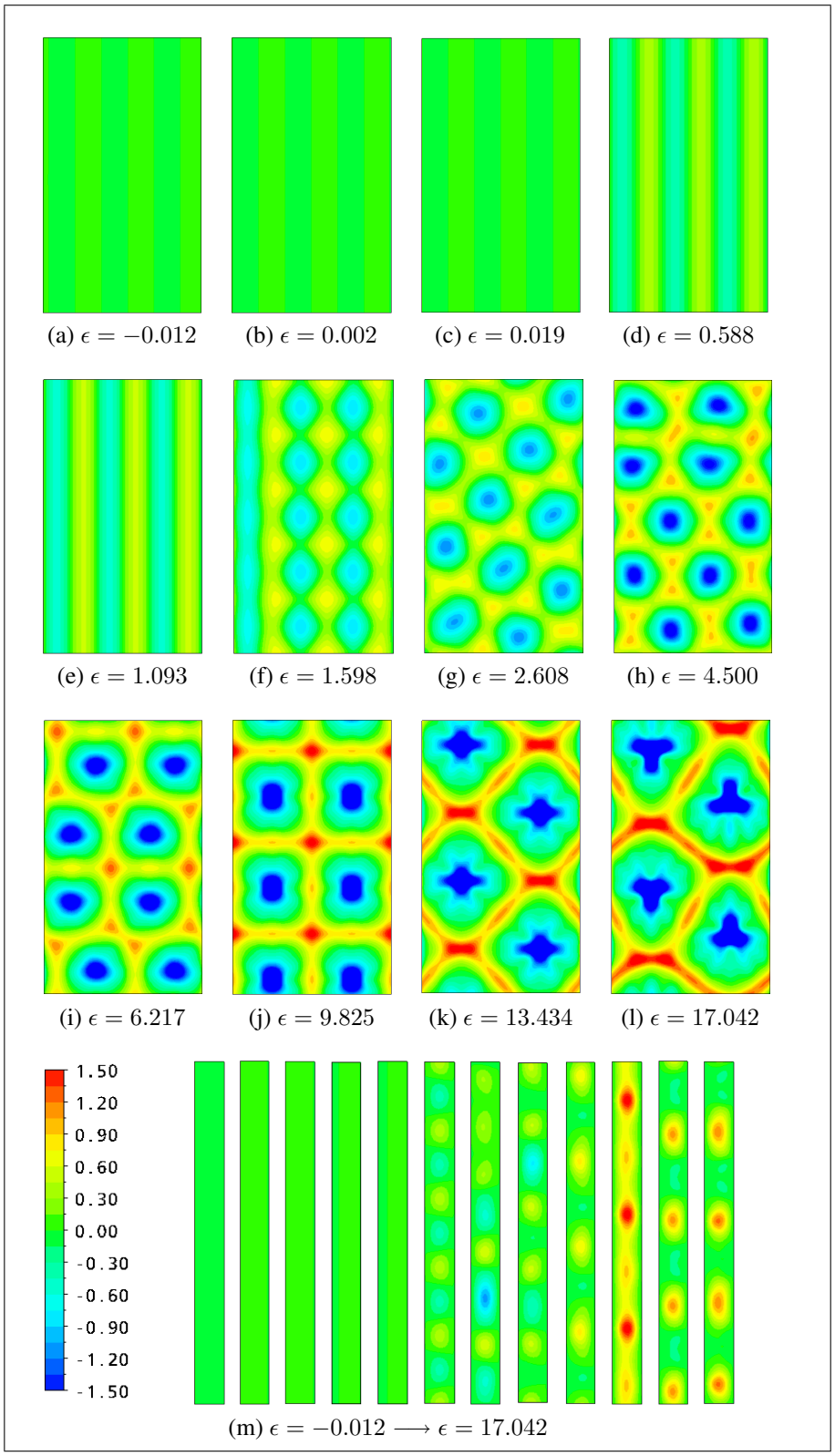

Figure 5: *u velocity component contours on the midlayer and spanwise planes in Figure 1.*

The modes plotted in Figure 3b correspond to the first six Fourier space modes. The first mode is associated with the z-axis rolls (see Figures 4b to 4e and 5b to 5e) that are observed in the range $0 < \epsilon < 1$ with the increase amplitude, which is relative to the maximum of all the observed frequencies. The first of three square circulation cell states (Figures 4f and 5f), the relative amplitude of the sixth mode is also significant (Figure 3b); thus according to linear theory this state should be associated with rolling waves in the y-axis direction.

The next states are observed at $\epsilon = 2.6$ where all of the six modes show some effect on the horizontal layer (Figure 3b). Examining both the temperature (Figures 4g & 4h) and u velocities (Figure 5g & 4h), hexagonal and several pentagonal circulation cells are observed. At $\epsilon = 2.6$ the first, third and fifth modes all have a similar relative amplitude whilst the second and sixth modes are within ± 0.08 of this amplitude and the fourth mode is quite different. However, at $\epsilon = 3.9$, the modes have a relative amplitude of 0.13 ± 0.03 except for the third mode. Whilst at $\epsilon = 4.5$ and 4.7, the modes are arranged into two groups at relative amplitudes of 0.17 ± 0.06 for the first, second and fifth modes and at 0.50 ± 0.07 for the remaining modes.

At $\epsilon = 6.2$, there is a spread of the modes, where what seems to be distorted pentagons (Figures 4i & 5i) are the only circulation cells present. At this point the relative amplitude of the third and sixth modes become insignificant when compared to the other four modes.

At $\epsilon \approx 10$ a second square state is formed (Figures 4j & 5j), but this state varies in orientation and also the modes that characterise its behaviour (i.e. modes 1 and 4 rather than modes 1 and 6). A third square state is formed at $\epsilon > 13$ (Figures 4k & 4l with 5k & 5l), where again the orientation of the cells is changed and the significant modes are the first and third modes whilst the fourth and sixth modes are insignificant. However, in this case spokes are formed within the circulation cell. As ϵ is increased towards the transient regime, the square circulation cell is stretched along the z-axis, which can be associated with either the first or the fifth mode (Figure 3b).

Both Groh et al. (2007) and Thiele and Eckert (1998) categorised the evolution of circulation cells from hexagons to other structures via two distinct methods, as previously mentioned Groh et al. (2007) examined the Fourier space modes whilst Thiele and Eckert (1998) used a stochastic geometrical method to identify the different structures. However, in the case of Groh et al. (2007) only rolls were formed from the stretching of the hexagons as magnetic fields were altered. Thiele and Eckert (1998) showed that both hexagons and pentagons could coexist in a *Bénard-Marangoni* layer via analysis of the vertices of the circulations cells. It was also shown that the state could change from hexagonal cells to pentagons then to squares through the loss of one or two of these vertices. These vertices could be considered equivalent to the Fourier space modes, which have been used here to identify or categorise the different circulation cells predicted by the simulations performed here. However, in the case of Thiele and Eckert (1998) the patterns were initially hexagonal before reduction in the significance of one or two of the vertices, whilst in the current study the initial patterns were z-axis rolls followed by squares, then hexagons and pentagons and then back to squares as the importance of the different modes changed with the increase in ϵ.

Nevertheless, hexagonal cells are the preferred mode for the instability evolution of homogeneous systems. In the case where there is no isotropy breaking, rolls seem to be the preferred mode of evolution; however, when breaking of isotropy is introduced, for example via a temperature dependence of material properties such as viscosity (Busse, 1967), then the importance of the rolls diminishes as the magnitude of the isotropy breaking term increases.

In our work here, we have considered the case where the boundary conditions were not symmetric and an additional heat flux was applied homogeneously. Our numerical studies have shown that for Prandtl numbers of O(10), the preferred mode of instability is hexagons. Work to identify the stability characteristics as a function of the Grashof and wave numbers is on-going. In addition, further studies have been performed that examined the instability of internally heated layers of fixed depth that are rigid, conducting or insulating boundaries (Generalis and Busse, 2008). The effect that a pressure gradient has on the circulation cells that were generated has also been investigated.

Acknowledgements

We wish to thank the Institute for Safety Research at the Forschungszentrum Dresden-Rossendorf for kindly allowing access to the computational cluster at the Forschungszentrum Dresden-Rossendorf upon which the calculations were performed. We would also like to thank Roman Vaibar for his assistance in the application of the fast Fourier transforms.

References

ANSYS, 2007, ANSYS CFX 11. ANSYS Inc., Canonsburg, PA, USA.

Arter, W., Bernoff, A., and Newell, A. C., 1987, Wavenumber selection of convection rolls in a box, Physics Fluids, 12(12), 3840–3842.

Asfia, F. J. and Dhir, V. K., 1996, An experimental study of natural convection in a volumetrically heated spherical pool bounded on top with a rigid wall, Nuclear Engineering Design, 163, 333–348.

Busse, F. H., 1967, The stability of finite amplitude cellular convection and its relation to an extremum principle, J. Fluid Mechanics, 30(4), 625–649.

Generalis, S. and Nagata, M., 2003, Transition in homogeneously heated inclined plane parallel shear flows, J. Heat Transfer, 125, 795–803.

Generalis, S. C. and Busse, F. H., 2008, In Proceedings of the 5th European Thermal-Sciences Conference, number 74, Eindhoven.

Gershuni, G. Z., Zhukhovitsky, E. M., and Yakimov, A. A., 1974, On stability of plane-parallel convective motion due internal heat sources, Int. J. Heat Mass Transfer, 17, 717–726.

Groh, C., Richter, R., Rehberg, I., and Busse, F. H., 2007, Reorientation of a hexagonal pattern under broken symmetry: The hexagon flip, PHYSICAL REVIEW E, 76, 055301(R).

Houseman, G., 1988, The dependence of convection planform on mode of heating, Nature, 332, 346–349.

Ichikawa, H., Kurita, K., Yamagishi, Y., and Yanagisawa, T., 2006, Cell pattern of thermal convection induced by internal heating, Physics Fluids, 18, 038101.

Roberts, P. H., 1967, Convection in horizontal layers with internal heat generation. theory., J. Fluid Mechanics, 30(1), 33–49.

Schmalzl, J., Houseman, G. A., and Hansen, U., 1995, Mixing properties of three-dimensional (3-d) stationary convection, Physics Fluids, 7(5), 1027–1033.

Schubert, G., Glatzmaier, G. A., and Travis, B., 1993, Steady, three-dimensional, internally heated convection, Physics Fluids, 5(8), 1928–1932.

Thiele, U. and Eckert, K., 1998, Stochastic geometry of polygonal networks: An alternative approach to the hexagon-square transition in benard convection, Physical Review E, 58(3), 3458–3468.

Tritton, D. J. and Zarraga, M. N., 1967, Convection in horizontal layers with internal heat generation, J. Fluid Mechanics, 30(1), 21–31.

Tveitereid, M. and Palm, E., 1976, Convection due to internal heat sources, J. Fluid Mechanics, 76, 481–499.